Metals & corrosion

Cellular automata coupled finite element simulation for dynamic recrystallization of extruded AZ80A magnesium alloy

Xingwang Duan[1,*] , Min Wang[1], Xin Che[1], Linfeng He[1], and Jiachen Liu[1,2]

[1] College of Materials Science and Engineering, Taiyuan University of Science and Technology, Taiyuan 030024, People's Republic of China
[2] Materials Research and Education Center, Auburn University, Auburn, AL 36849, USA

ABSTRACT

The dynamic recrystallization (DRX) behavior of the extruded AZ80A magnesium alloy during plastic deformation was studied by coupling the physical-based finite element (FE) method and the developed cellular automata (CA) model. Isothermal compression tests were conducted by Gleeble-3800 thermal simulator at different temperatures of 598 K, 623 K, 648 K, 673 K, 698 K, and 723 K, and different strain rates of $0.001\ s^{-1}$, $0.01\ s^{-1}$, $0.1\ s^{-1}$, and $1\ s^{-1}$ to obtain the corresponding flow stress–strain curves. The constitutive model was established based on the analysis of the flow stress–strain curves. Moreover, parameters of the CA model were found. Based on the CA model, the DRX model was built. The established constitutive model and the DRX model were embedded in DEFORM-3D software to simulate the grain evolution under various deformation conditions. This combined method was capable of predicting the evolution of flow stress, DRX volume fraction, and DRX grain size in various deformation conditions. The results show that the error between the recrystallization volume fraction predicted by the finite element simulation and the CA model and the experimental results is less than 12.0%, and the error between the peak stress predicted by the CA model and the measured value remains within 8.0%. The prediction results of the combined methodology of the CA model and the FE simulation are consistent with the experimental results, which verify the usefulness and the prediction prospect of the coupled method. This method was probably a feasible choice to predict the DRX grain refinement of the thermal deformation process of the extruded AZ80A magnesium alloy.

🙌 Springer

GRAPHICAL ABSTRACT

The dynamic recrystallization (DRX) behavior of the extruded AZ80A magnesium alloy during plastic deformation was studied by coupling the physical-based finite element (FE) method and the developed cellular automata (CA) model. The results show that the error between the recrystallization volume fraction predicted by the finite element simulation and the CA model and the experimental results is less than 12.0%, and the error between the peak stress predicted by the CA model and the measured value remains within 8.0%.
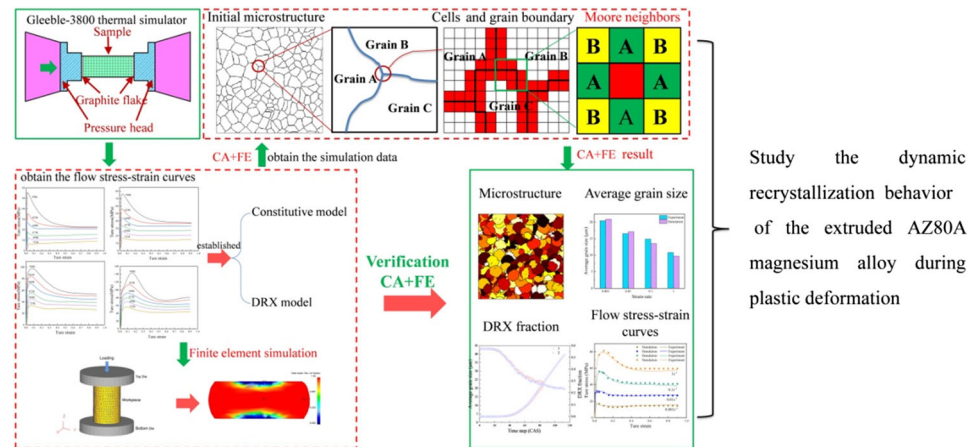
Introduction

With the increasing prominence of the energy crisis, magnesium alloys have been widely used for lightweight structural parts due to their low density, high specific stiffness, high specific strength, superior shock absorption, and other advantages, which are crucial to the development of the lightweight spacecraft and vehicles [1, 2]. Due to the high density of the hexagonal structures, fewer slip systems, and low stacking fault energy, magnesium alloys have poor plastic deformation ability at room temperature, which limits their application in the industry. Therefore, thermoplastic deformation has become a common method to shape structural parts made of magnesium alloys. Dynamic recrystallization (DRX) is more likely to occur under high-temperature deformation conditions, which in turn controls the microstructure evolution of magnesium alloys to make a better comprehensive performance after the plastic deformation [3]. Therefore, studying the plastic deformation behavior of magnesium alloys at high temperatures to improve the performance and material efficiency of the structural parts made of magnesium alloys attracts much attention.

In recent years, although studies on DRX never stopped, the microstructure and mechanical properties of the materials are mainly focused on mechanical processing methods such as thermal compression and tension [4]. As has been well known, DRX is not only an important physical metallurgical phenomenon but also an important means of grain refinement. It is found that the development of DRX can improve the plastic formability of magnesium alloys [5]. The DRX process of the metal alloys can be divided into two mechanisms: continuous dynamic recrystallization (CDRX) and discontinuous dynamic recrystallization (DDRX) [6]. CDRX mainly occurs in high-level fault energy materials such as aluminum. In the thermal deformation process, the subgrain boundary continuously absorbs dislocations, which changes the small-angle subgrain into the large-angle grain. This process

is developed by consuming dislocation density and reducing overall distortion energy, resulting in grain refinement [7]. The evolution process of DDRX mainly occurs in materials with medium and low stacking fault energy, such as copper. This process can be realized by the migration of large-angle grain boundaries, which is consistent with the traditional DRX mechanism to eliminate dislocations and subgrain boundaries in the deformed matrix through nucleation and growth of the recrystallized grains [8]. However, the evolution process of DRX is very complex, dynamic, and random. Experimental methods and physics-based models can partially reflect some of the internal processes, but barely very well predict the microstructural evolution. A prediction of the dynamic microstructural evolution faces more difficulty.

However, a combination of numerical calculations and material parameters provides a different approach to simulating DRX behavior. Some models are used to predict the microstructural evolution of different materials in DRX behavior. At present, the main simulation methods include the Monte Carlo method, phase-field method, and cellular automata method. The Monte Carlo method cannot directly reflect the migration mechanism of grain boundaries [9]. The phase-field method has the largest amount of calculation among these methods [10]. In contrast, the cellular automata (CA) method has many advantages in the simulation of the nucleation and growth of recrystallized grains [11, 12]. In addition, CA not only simplifies the model but also improves computational efficiency [13]. CA method has been increasingly used for simulation in recent years. DING and GUO [14] proposed a two-dimensional model that combined the DRX metallurgical principle with CA and successfully simulated the grain growth direction and the shape of pure copper. The results show that the initial microstructure also has a certain influence on DRX behavior. Subsequently, CA was widely used to simulate various materials. Han et al. [15] established a DRX-CA model, which revealed its unsuitability at high strain rates and successfully simulated and predicted the dynamics of recrystallization behavior of titanium alloys. Chen et al. [16] proposed a method to predict microstructural evolution by tracking dislocation density and used an updated topological deformation technique to study the DRX behavior of austenitic stainless steels.

Coupling the CA model and finite element (FE) method can more reliably predict grain refinement developed by the DRX process due to a consideration of the physical mechanism of the DRX process. Li et al. [17] built the CA algorithm of DRX evolution into the CPFEM framework and made a good prediction of multi-scale non-uniform deformation, mechanical response, and microstructural evolution of titanium alloy, but the double calculation is required in the coupling process, resulting in difficulties in calculation and coding. Wang et al. [18] simulated the microstructural evolution during hot compression of homogenized 5052 aluminum alloy and AZ31 magnesium alloy using a CA coupled FE method, showing that a larger degree of deformation leads to grain refinement. Lee et al. [19] obtained local data for the input parameters of CA simulation through FE analysis. They simulated the dynamic recrystallization behavior of pure copper and successfully simulated the hot gear blank forging process by using this model. Jaeger et al. [20] proposed to couple two 3D models of crystal plasticity FE method and recrystallization process. Compared with previous simulation methods, the current model took into account the volume of the sample and successfully predicted the stress field and strain field, the evolution of energy storage, and the local crystallographic orientation of superalloys. In summary, many scholars have studied it and obtained corresponding results, which are mainly used to predict the microstructure of various materials. However, there are barely studies on the DRX behavior of the extruded AZ80A magnesium alloy using the coupling physics-based FE method and the CA model. In particular, the prediction of the microstructural evolution of this material has not been found.

In this research, the DRX behavior of the extruded AZ80A magnesium alloy in different temperatures and strain rates was studied by hot compression experiments. The established DRX dynamic model and constitutive model were incorporated into a FE simulation platform, DEFORM-3D software. A two-dimensional CA model was also used to study the microstructural evolution and the relationship between microstructure and deformation parameters during the thermal deformation processes.

Materials and experiment procedures

Cylindrical samples with a size of Φ10mm × 15 mm were processed from the solution-treated extruded AZ80A magnesium alloy bars. The chemical

Table 1 Chemical composition of the extruded AZ80A magnesium alloy (wt.%)

Element	Al	Zn	Mn	Si	Fe	Cu	Ni	Mg
Content	8.50	0.60	0.30	0.021	0.003	0.01	0.001	Ba

compositions (mass fraction %) are shown in Table 1. The microstructure of the homogenized extruded AZ80A magnesium alloy with an average grain size of 43.33 μm is shown in Fig. 1a. Isothermal compression tests were carried out on Gleeble-3800 thermal simulator under different temperatures of 598 K, 623 K, 648 K, 673 K, 698 K, and 723 K, and strain rates of 0.001 s^{-1}, 0.01 s^{-1}, 0.1 s^{-1}, 1 s^{-1}, and a compression ratio of 60% which corresponds to a true strain of 0.916. Before compressing the sample, to reduce friction, graphite sheets were placed at both ends of the sample and coated with lubricating oil. The hot deformation process diagram is shown in Fig. 1b, and the deformation testing diagram is shown in Fig. 1c. Each sample was heated to the corresponding temperature at the speed of 10 K · s^{-1}, and the compression test was carried out after a holding of the temperature for 180 s. After compression, the sample was immediately water quenched to freeze the microstructure. The compressed sample was cut along the cross section parallel to the compression direction. Polish and etch were followed. The microstructure in the middle of the sample was observed by an optical microscope (OM). The average grain size and recrystallization fraction of the compressed sample were calculated and simulated. EBSD data were obtained by Oxford Symmetry electron backscatter diffraction detector.

Experimental results

True stress–strain curve

Figure 2 shows the true stress–strain curves of the extruded AZ80A magnesium alloy under the temperature of 598–723 K and the strain rate of 0.001–1 s^{-1}. The flow stress increases with the decrease in the deformation temperature and the increase in the strain rate, indicating that the flow stress is sensitive to the temperature and strain rate. At the beginning of hot deformation, the increase in the dislocation density leads to work hardening, and the flow stress increases monotonically with the increase in the work hardening. After reaching the peak of the flow stress curve, a decrease in the flow stress can be observed. The reason is that, with the development of recrystallization mainly caused by dislocation climbing, the effect of dynamic softening

Figure 1 **a** Microstructure of homogenization treated extruded AZ80A magnesium alloy; **b** diagram of the hot deformation process of the extruded AZ80A magnesium alloy; **c** deformation testing.
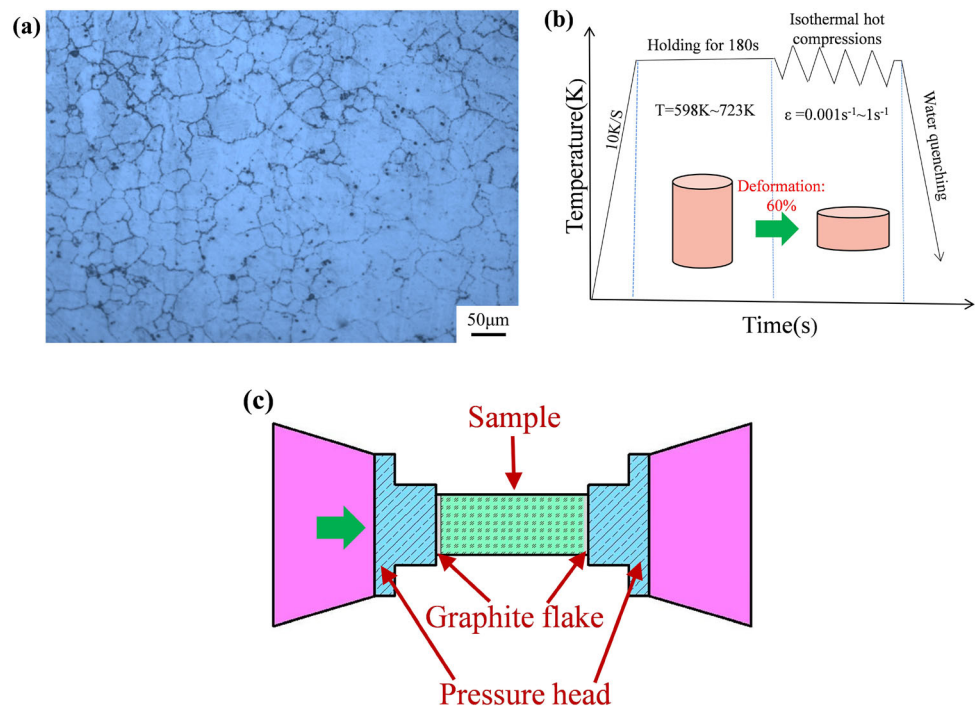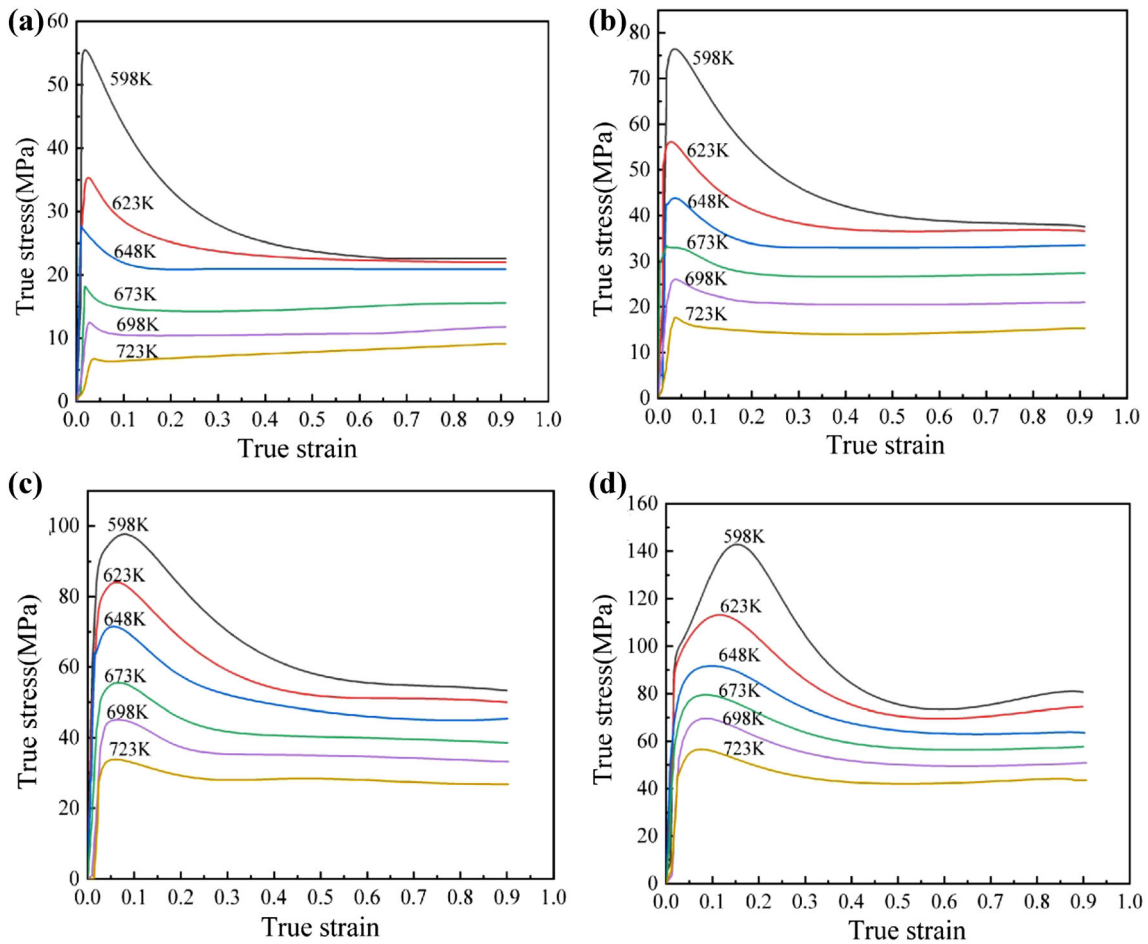
Figure 2 Stress–strain curves of the extruded AZ80A magnesium alloy under different deformation conditions: **a** 0.001 s^{-1}; **b** 0.01 s^{-1}; **c** 0.1 s^{-1}; **d** 1 s^{-1}.

is greater than the effect of work hardening. After deformation, the work hardening and dynamic softening reach a balance, and the flow stress reaches a stable state. In the initial stage of deformation, the stress increases with the increase in the deformation and reaches a certain peak value of σ_P (the strain deformation corresponding to this stress is ε_p), and the yield stress drops again to a certain constant value of σ_{ss} due to DRX.

Constitutive model

The experimental results in Fig. 2 show that the flow stress mainly depends on the deformation temperature and the strain rate, and the modified hyperbolic Arrhenius function can better describe the

relationship between them. In general, the constitutive model can be expressed by the following formula [21]:
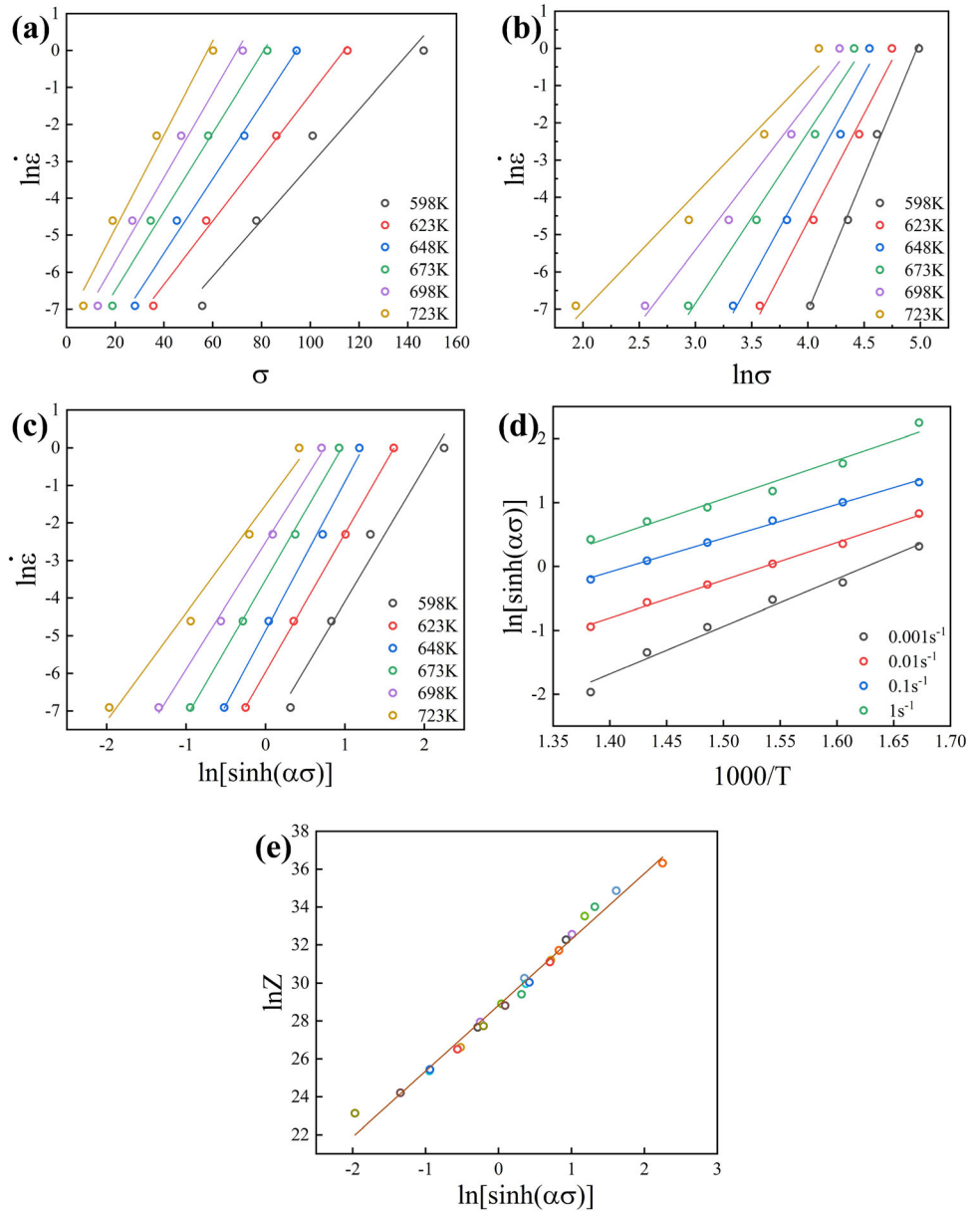
$$\dot{\varepsilon} = A_1 \sigma^{n_1} \exp\left(-\frac{Q}{RT}\right) \tag{1}$$

$$\dot{\varepsilon} = A_2 \exp(\beta\sigma) \exp\left(-\frac{Q}{RT}\right) \tag{2}$$

$$\dot{\varepsilon} = A[\sinh(\alpha\sigma)]^n \exp\left(-\frac{Q}{RT}\right) \tag{3}$$

where A, A_1, A_2, α, β, n and n_1 are constants related to the material state, σ is the flow stress, Q is the activation energy of thermal deformation, and R is the molar gas constant.

Figure 3 **a** ln $\dot{\varepsilon}$–σ curve; **b** ln $\dot{\varepsilon}$–ln σ curve; **c** ln $\dot{\varepsilon}$–ln[sinh($\alpha\sigma$)] curve; **d** ln[sinh($\alpha\sigma$)]–1000/T curve; **e** ln$Z$–ln[sinh($\alpha\sigma$)] curve.

α can be obtained as 0.0201 by the following formula, in which β and n_1 can be obtained according to the slope fitting in Fig. 3a, b:

$$\alpha = \beta/n_1 = \left(\frac{\partial \ln \dot{\varepsilon}}{\partial \sigma}\right) \Big/ \left(\frac{\partial \ln \dot{\varepsilon}}{\partial \ln \sigma}\right) \tag{4}$$

At the thermal deformation temperature, there is a functional relationship between the strain rate $\dot{\varepsilon}$ and the stress σ, so the Z parameter is introduced [22, 23]:

$$Z = \dot{\varepsilon}\exp\left(-\frac{Q}{RT}\right) = A[\sinh(\alpha\sigma)]^n \tag{5}$$

Taking the logarithm of both sides of Eq. (3), we get Eq. (6)

$$\ln \dot{\varepsilon} = \ln A + n\ln[\sinh(\alpha\sigma)] - \frac{Q}{RT} \tag{6}$$

n and Q can be expressed as:

$$n = \frac{\partial \ln \dot{\varepsilon}}{\partial \ln[\sinh(\alpha\sigma)]} \tag{7}$$

$$Q = RnM = R\left[\frac{\partial \ln \dot{\varepsilon}}{\partial \ln[\sinh(\alpha\sigma)]}\right]_T \left[\frac{\partial \ln[\sinh(\alpha\sigma)]}{\partial(1000/T)}\right]_{\dot{\varepsilon}} \tag{8}$$

The value of n according to Eq. (7) is the average of the slope of the ln $\dot{\varepsilon}$– ln[sinh($\alpha\sigma$)] curve, as shown in

Fig. 3c. The value of n is 3.52062. The value of M can be obtained by fitting the curve $\ln[\sinh(\alpha\sigma)] - 1000/T$. At the same time, according to Eq. (8), the value of Q is 180000 J/mol and the value of A is 3.30984×10^{12}, which are obtained from the intercept of $\ln Z - \ln[\sinh(\alpha\sigma)]$ curve, as shown in Fig. 3d, e.

To sum up, the constitutive model of the extruded AZ80A magnesium alloy can be expressed as:

$$\dot{\varepsilon} = 3.30984 \times 10^{12}[\sinh(0.0201\sigma)]^{3.52062}\exp\left(-\frac{180000}{RT}\right) \tag{9}$$

DRX kinetic model

During the process of thermoplastic deformation, DRX occurs when the increased dislocation density reaches the critical dislocation density and the DRX volume fraction gradually increases. Most of them are related to critical strain and temperature, which can be characterized by DRX kinetic equation [24, 25].

$$X_{DRX} = 1 - \exp\left[-k\left(\frac{\varepsilon - \varepsilon_c}{\varepsilon_p}\right)^m\right](\varepsilon \geq \varepsilon_c) \tag{10}$$

where X_{DRX} is the volume fraction of DRX, ε_p is the peak strain (corresponding to σ_p), and k and m are material constants.

At the same time, the volume fraction of dynamic recrystallization can be expressed as [26, 27];

$$X_{DRX} = \frac{\sigma_p - \sigma}{\sigma_p - \sigma_{ss}} \tag{11}$$

where σ_p is the peak stress and σ_{ss} is the steady-state stress.

Taking the logarithm of both sides of Eq. (10), we get

$$\ln[-\ln(1 - X_{DRX})] = \ln k + m\ln[(\varepsilon - \varepsilon_c)/\varepsilon_p] \tag{12}$$

The DRX volume fraction can be calculated from Eq. (11), and the values of m and k can be obtained by a linear fitting between $\ln[-\ln(1 - X_{DRX})]$ and $\ln[(\varepsilon - \varepsilon_c)/\varepsilon_p]$. The slope of the fitted straight line is m and the intercept is $\ln k$, which are calculated to be 2.756 and -0.17406, respectively. Therefore, the extruded AZ80A magnesium alloy based on DRX kinetics can be expressed as follows:
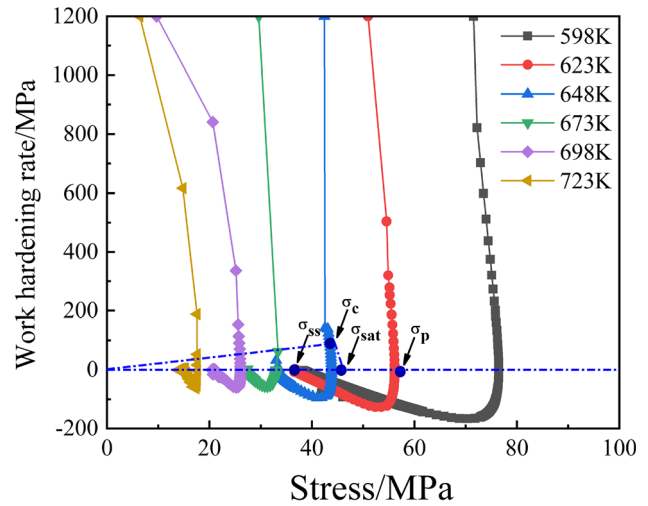

Figure 4 θ–σ curves for different temperatures and a strain rate of 0.01 s^{-1}.

$$\begin{cases} X_{DRX} = 0 & (\varepsilon \leq \varepsilon_c) \\ X_{DRX} = 1 - \exp\left[-0.17406\left(\frac{\varepsilon - \varepsilon_c}{\varepsilon_p}\right)^{2.0756}\right] & (\varepsilon \geq \varepsilon_c) \end{cases} \tag{13}$$

Determination of simulation parameters

In the establishment of the DRX model based on CA, some deformation and non-deformation parameters need to be determined before they can be simulated. The deformation parameters are mainly obtained from the stress–strain curve obtained by the thermal compression test. The Zener–Hollomon (Z) correlation function can be established by the corresponding linear fittings and calculations of some parameters [28], as can be expressed below:

$$Z = \dot{\varepsilon}\exp\left(-\frac{Q}{RT}\right) \tag{14}$$

Through the relationship between the work hardening rate θ and the flow stress at different temperatures and a strain rate of 0.01 s^{-1} in Fig. 4, the steady-state stress (σ_{ss}), peak stress (σ_p), critical stress (σ_c), and saturation stress (σ_{sal}) under various deformation conditions can be obtained. By linear fitting to the experimental results, the value of ε_c can be represented by 0.6334 ε_p. Moreover, ε_p, σ_{ss}, and σ_{sal} can be expressed as a function of the Zener–Hollomon (Z) parameter, respectively, as shown in Fig. 5.
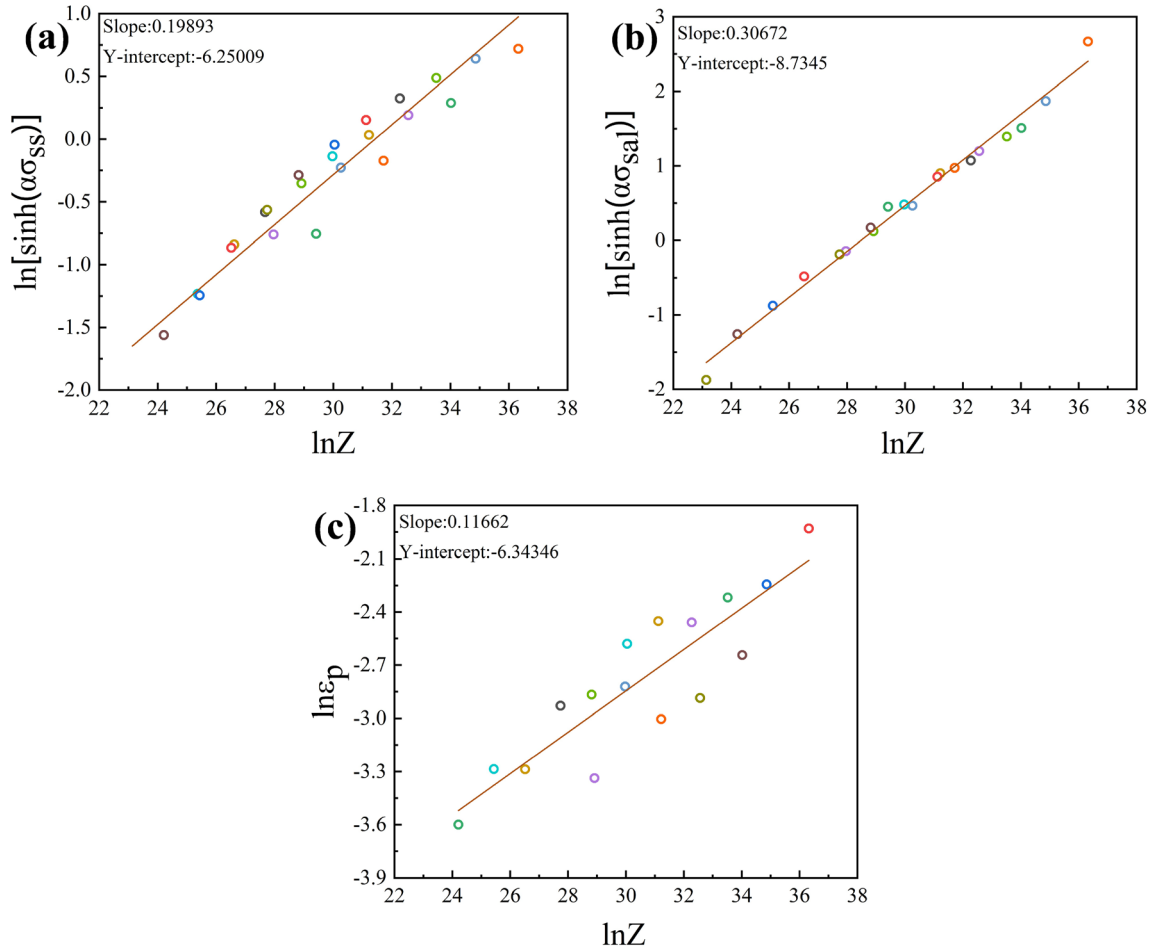
Figure 5 **a** $\ln Z$–$\ln[\sinh(\alpha\sigma_{ss})]$ curve; **b** $\ln Z$–$\ln[\sinh(\alpha\sigma_{sal})]$ curve; **c** $\ln Z$–$\ln \varepsilon_p$ curve.

$$\varepsilon_c = 0.6334\varepsilon_p \tag{15}$$

$$\varepsilon_p = 0.00176Z^{0.11662} \tag{16}$$

$$\sigma_{ss} = 28.827792 \times \sinh^{-1}(0.0201Z^{0.19893}) \tag{17}$$

$$\sigma_{sal} = 28.827792 \times \sinh^{-1}(0.022Z^{0.30672}) \tag{18}$$

Numerical simulation

Finite element simulation and result analysis

Due to the friction between the sample and the punch during the hot compression process, the deformation in the sample is non-uniformly distributed. Therefore, to study the microstructure in different regions of the sample, the DEFORM-3D software based on the finite element (FE) method was used to simulate
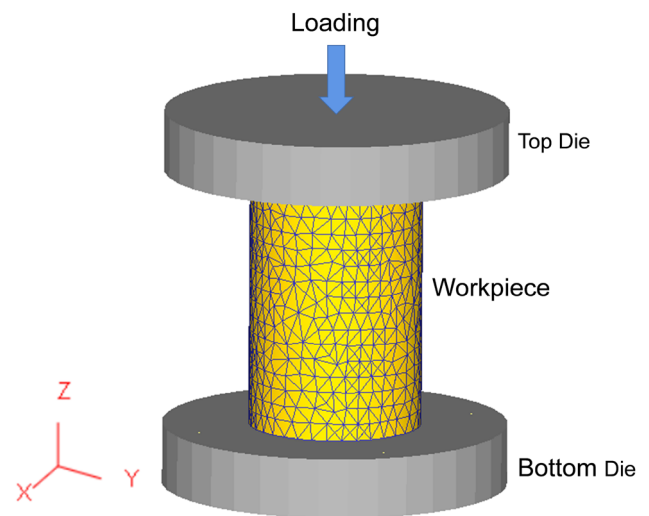

Figure 6 Finite element model for thermal compression simulation.

the hot compression process of the extruded AZ80A magnesium alloy under different deformation conditions.

Figure 6 shows the FE model for the simulation of the hot compression process. In the model, the sample is set as a plastic body. The top and bottom molds/dies are set as rigid bodies. During the process of hot compression, the lower die remains stationary and the load is applied to the upper die to compress the sample along the Z-axis. To better study the thermal deformation behavior of the material, the physical-based constitutive model and dynamic model of the extruded AZ80A magnesium alloy were embedded in the finite element analysis of the DEFORM-3D software.

Figure 7 shows the microstructure under different deformation conditions of the temperature of 623 K and 673 K and the strain rate of 0.01 s^{-1}, 0.1 s^{-1}, and 1 s^{-1}. At the same temperature (as shown in Fig. 7a, b or Fig. 7c, d), when the strain rate is 1 s^{-1}, the figure shows that no complete recrystallization has occurred, and a small number of initial grains can still be observed, while the initial grains are compressed and elongated. When the strain rate is 0.01 s^{-1}, it can be observed that there are many fine nucleation grains under this condition. At the same strain rate (Fig. 7a, c), when the temperature is 673 K,

compared with Fig. 7a, the recrystallized grains in Fig. 7c have grown significantly. The results show that, at the same temperature, the higher the strain rate, the smaller the recrystallization grain size and the more incomplete the recrystallization. The higher the temperature at the same strain rate, the larger the grain size and the more complete the recrystallization.

Figure 8 shows the DRX volume fraction under different deformation conditions simulated by the FE method. Comparing Fig. 8a and b, Fig. 8c, and d, respectively, at the same temperature, with the increase in the strain rate, the complete development of DRX can be observed in the middle region of the compressed sample. Comparing Fig. 8a and c, at the same strain rate, with the increase in temperature, the observation of the microstructure indicates that the development of the DRX in the middle region of the sample is more complete. The reason is that, under all deformation conditions, the DRX volume fraction of the difficult deformation areas near the contact surfaces between the sample and the dies is much smaller than that of the large deformation area in the middle of the sample due to friction. The large deformation area has a higher degree of the development of DRX, which is consistent with the experimental results. Therefore, the FE simulation method

Figure 7 Microstructure of the extruded AZ80A magnesium alloy under different deformation conditions: **a** 623 K, 0.01 s^{-1}; **b** 623 K, 1 s^{-1}; **c** 673 K, 0.01 s^{-1}; **d** 673 K, 0.1 s^{-1}.
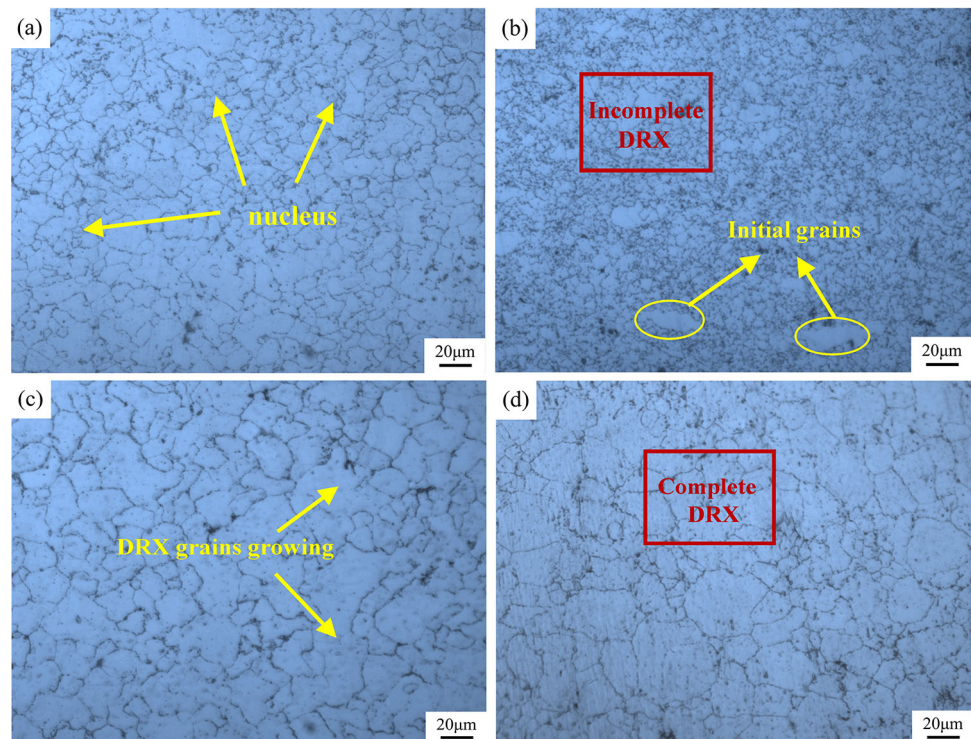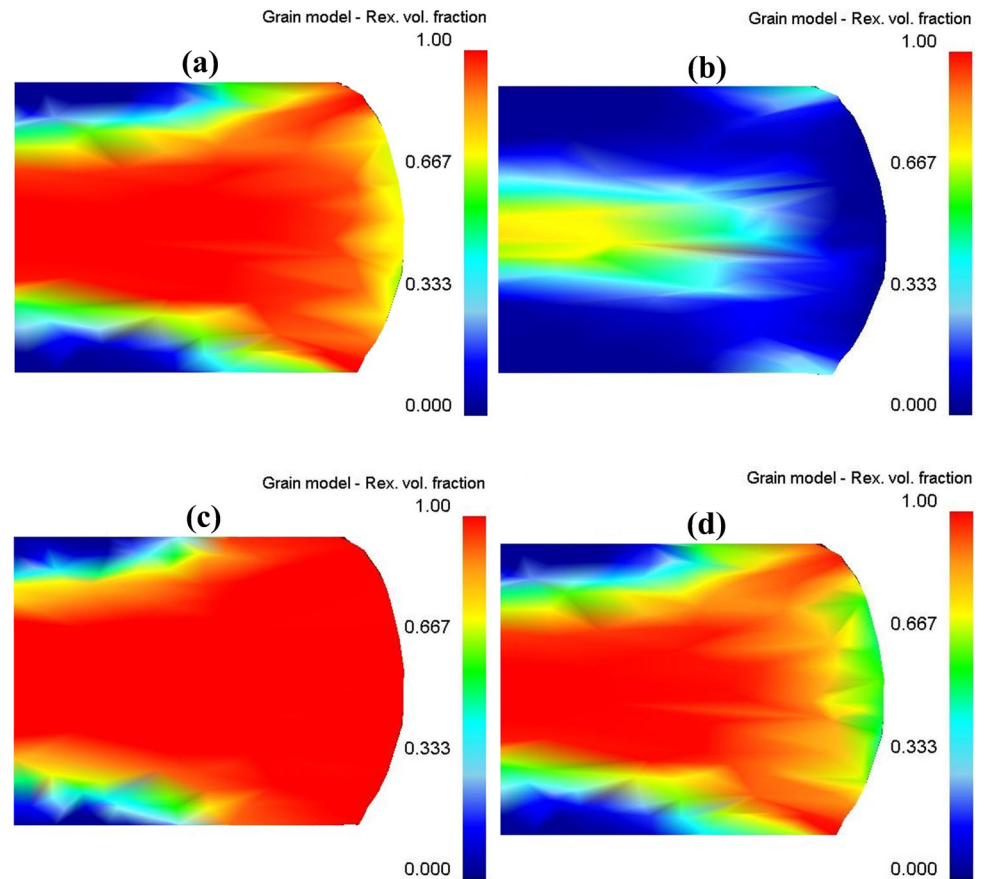
Figure 8 DRX volume fraction under different deformation conditions: **a** 623 K, 0.01 s^{-1}; **b** 623 K, 1 s^{-1}; **c** 673 K, 0.01 s^{-1}; **d** 673 K, 0.1 s^{-1}.

by DEFORM-3D can effectively predict the hot compression process of the extruded AZ80A magnesium alloy.

Figure 9 shows the microstructure diagram of different regions of the sample compressed at 673 K and 0.01 s^{-1}. To describe the deformation degree of different regions, the DRX volume fractions of different regions are compared with the experimental results calculated by the point tracking method. The larger the deformation degree of P1, the larger the DRX volume fraction, and the volume fraction is 100%. P2 shows the microstructure of the difficult deformation region, the DRX volume fraction by FE simulation is only 17%. P3 shows the microstructure of the medium deformation region, and the volume fraction of dynamic recrystallization is 100%. The errors between the finite element simulation results and the experimental results at points P1, P2, and P3 are 0, 11.2%, and 0.1%, respectively. The main reason for this phenomenon is that the degree of deformation in different regions is different, resulting in a change in the internal energy of the material during the thermal compression process. In summary, it reveals that the DRX volume fraction by FE simulation is in good agreement with the experimental result.

CA model

The plastic deformation of metals is mainly influenced by the interrelationship between work hardening and dynamic softening. In addition, the multiplication and annihilation of dislocations jointly affect the microstructural evolution. The CA model is composed of models of dislocation density, DRX nucleation, and grain growth. The CA model mainly relies on time and dimension discretization and transformation rules of adjacent cells and dynamically simulated microstructures.

Dislocation density evolution model

In the process of hot working, the evolution of dislocation density is mainly caused by work hardening, dynamic recovery, and dynamic recrystallization (DRX). Dislocation density plays an important role in recrystallization nucleation and growth. When the

Figure 9 Comparison of experimental and simulated DRX volume fractions of different deformation regions of the sample at 673 K and 0.01 s^{-1} and a true strain of 0.9.

Material point	DRX fraction(%)	
	Experiment	Simulation
P1	100	100
P2	15.2	17
P3	98.9	100
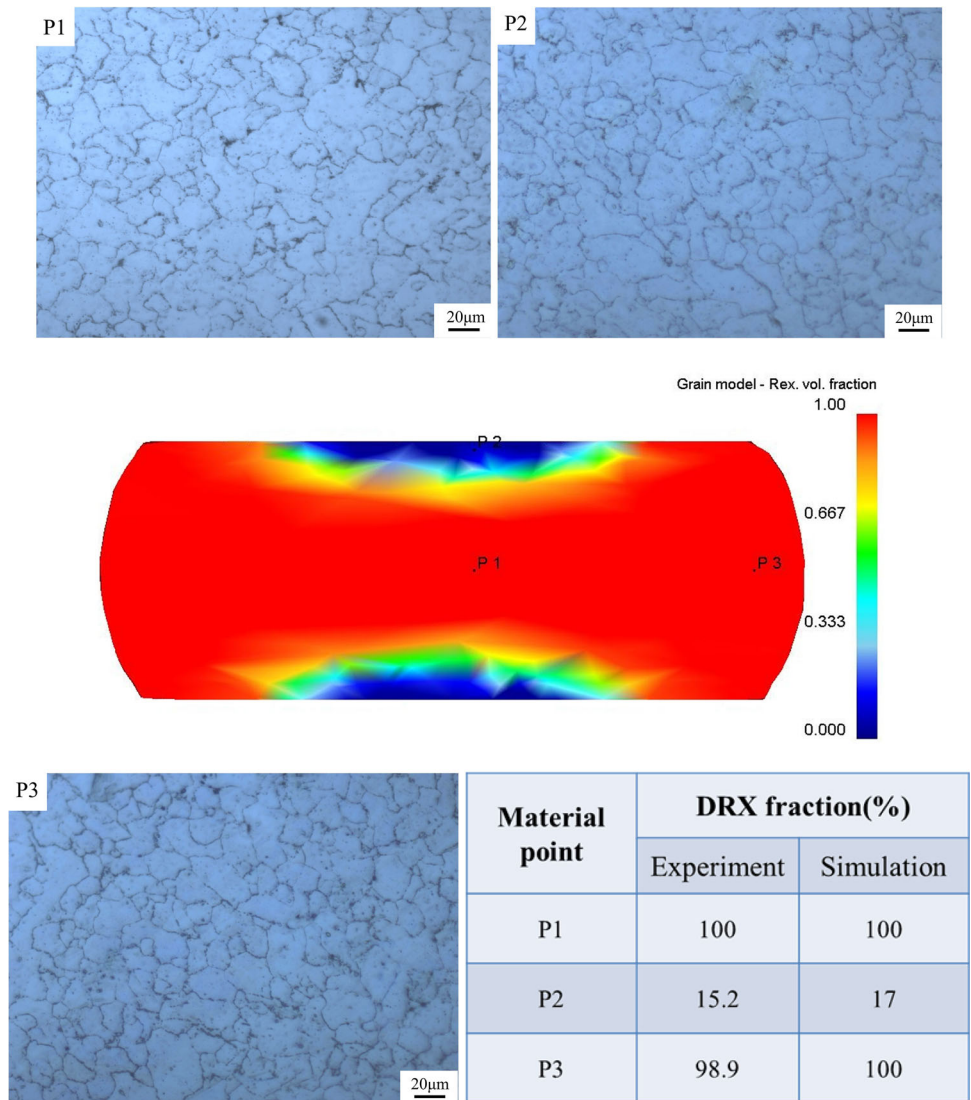
dislocation density reaches the critical strain corresponding to a dislocation density, DRX occurs. From the microscopic point of view, the dislocation density is generated by work hardening and eliminated by dynamic softening. Therefore, the KM dislocation density model proposed by Mecking and Kocks [29] is used to describe the evolution of dislocation density inside the grain, and the model is expressed below:

$$\frac{d\rho}{d\varepsilon} = k_1\sqrt{\rho} - k_2\rho \tag{19}$$

where k_1 and k_2 are the parameters related to work hardening and dynamic softening, which can be expressed by Eqs. (20) and (21), and the combined effect of work hardening and dynamic softening affects the dislocation density.

$$k_1 = \frac{2\theta}{\alpha Gb} \tag{20}$$

$$k_2 = \frac{2\theta}{\sigma_s} \tag{21}$$

where θ is the work hardening rate; G is the shear modulus.

The relationship between flow stress and average dislocation density can be expressed as follows [30]:

$$\sigma = \alpha Gb\sqrt{\overline{\rho}} \tag{22}$$

Table 2 Material parameters of the extruded AZ80A magnesium alloy

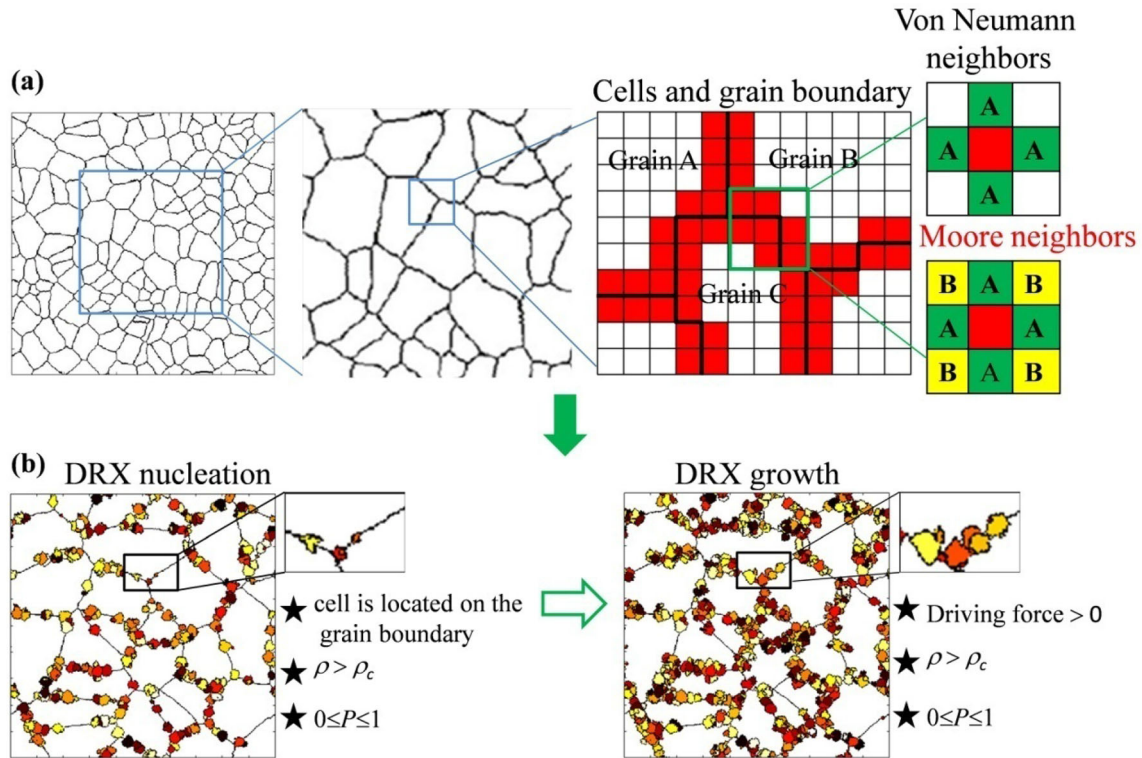| Parameter	δD_{ob} (m³ s⁻¹)	b (m)	μ (Pa)	v	Q (J/mol)	R
Value	5.0×10^{-12}	3.21×10^{-10}	1.75×10^{10}	0.33	180,000	8.314

Figure 10 Probabilistic cellular automata model simulates microstructure evolution: **a** predicted image of initially nucleated grains, **b** DRX nucleation, and growth.

where b is the Berger vector and $\overline{\rho}$ is the average dislocation density, which is the average dislocation density of all grains in the cell space.

Nucleation model

It is well known that DRX nucleation occurs when the dislocation density reaches a critical level. At present, there are various nucleation models; KURTZ [31] proposed a nucleation equation, which takes into account the strain rate and the nucleation rate:

$$\dot{n}(\dot{\varepsilon}, T) = C\dot{\varepsilon}^m \exp\left(-\frac{Q}{RT}\right) \qquad (23)$$

where $\dot{n}(\dot{\varepsilon}, T)$ is the nucleation rate; Q is the activation energy of thermal deformation; and C is the

nucleation rate constant, which can be obtained by inverse analysis [16, 32].

The nucleation is related to the accumulation mechanism of dislocation density at grain boundaries. When the DRX nucleation occurs, the dislocation density of the nucleated DRX grains returns to the initial state. According to Roberts and Ahlbom [33], the condition of the DRX nucleation is that the critical dislocation density (ρ_c) exceeds the threshold, and the critical dislocation density can be expressed:

$$\rho_c = \left(\frac{20\gamma_i \dot{\varepsilon}}{3blM\tau^2}\right) \qquad (24)$$

where l is the average degree of dislocation freedom; τ is the unit dislocation line energy, which can be expressed as $\tau = \mu b^2/2$; and γ_i is the grain boundary

Figure 11 DRX flowchart of the CA model simulation during isothermal compression.
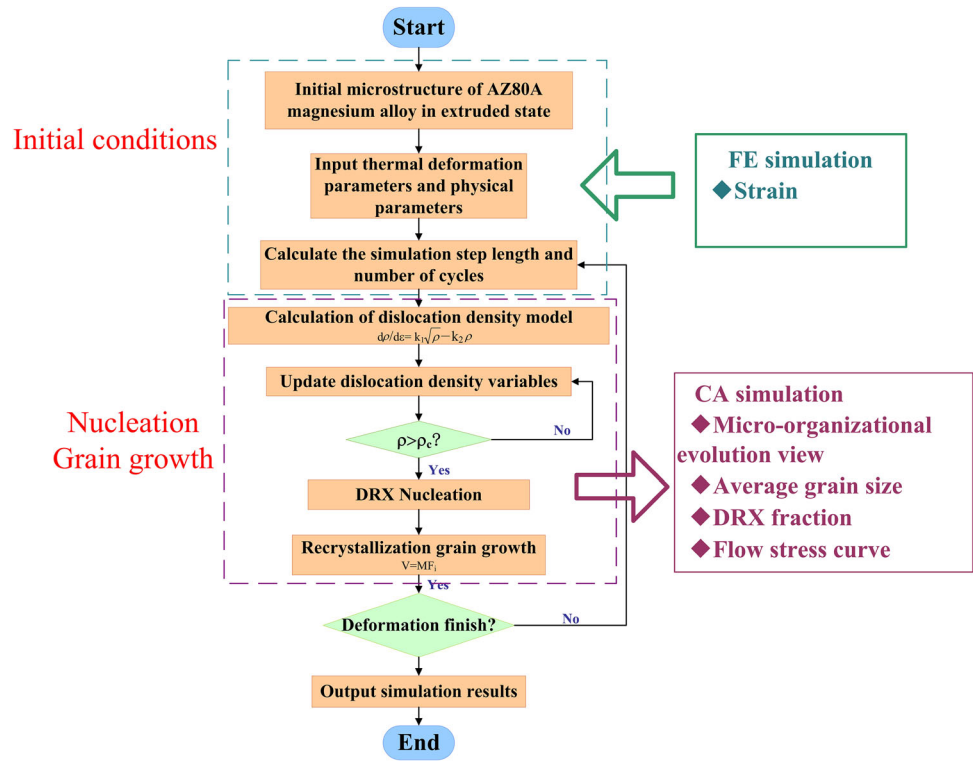
energy per unit area, and the calculation formula is as follows [34]:

$$\gamma_i = \begin{cases} \gamma_m & (\theta_i \geq 15°) \\ \gamma_m \dfrac{\theta_i}{\theta_m}\left[1 - \ln\left(\dfrac{\theta_i}{\theta_m}\right)\right] & (\theta_i < 15°) \end{cases} \quad (25)$$

where θ_i is the grain orientation difference between the ith recrystallized grain and the surrounding grains; and γ_i and θ_m represent the grain boundary energy and grain boundary orientation difference of the large-angle grains, respectively (take as 15°). γ_m can be obtained by Eq. (26) [16]:

$$\gamma_m = \frac{\mu b \theta_m}{4\pi(1-v)} \quad (26)$$

where v is Poisson's ratio.

Grain growth model

In the process of thermal deformation, when the dislocation density reaches a critical value, recrystallized grains nucleate. The difference in the dislocation density between the newly generated grains and the matrix provides the driving force for the growth of the recrystallized grains. Therefore, the grain growth rate can be expressed [35]:

$$V = MF_i/4\pi r^2$$
$$= \left[\frac{\delta D_{ob} b}{k_2 T}\exp\left(-\frac{Q_b}{RT}\right)\right]\left[\tau(\rho_m - \rho_i) - \frac{4\gamma_i}{d_i}\right]\Big/4\pi r^2 \quad (27)$$

where M is the grain boundary mobility; F_i is the driving force for the growth of each recrystallized grain; δ is the grain boundary thickness; D_{ob} represents the self-diffusion coefficient of the grain boundary; Q_b is the activation energy of grain boundary migration; K is the Boltzmann constant; ρ_m is the dislocation density in the parent phase; ρ_i is the dislocation density of the ith new grain; and d_i is the average diameter of the recrystallized grain.

In the simulation, the time step, Δt, can be represented by the cell diameter, l_0, and the maximum rate of grain boundary migration, v_{max}, as follows [34]:

$$\Delta t = \frac{l_0}{v_{max}} = \frac{k_2^2 l_0}{M\tau k_1^2} \quad (28)$$

The increment of strain can be expressed by $\Delta\varepsilon = \dot{\varepsilon}\Delta t$.

Cellular automata simulation

To better predict the microstructure of the extruded AZ80A magnesium alloy during plastic deformation, the
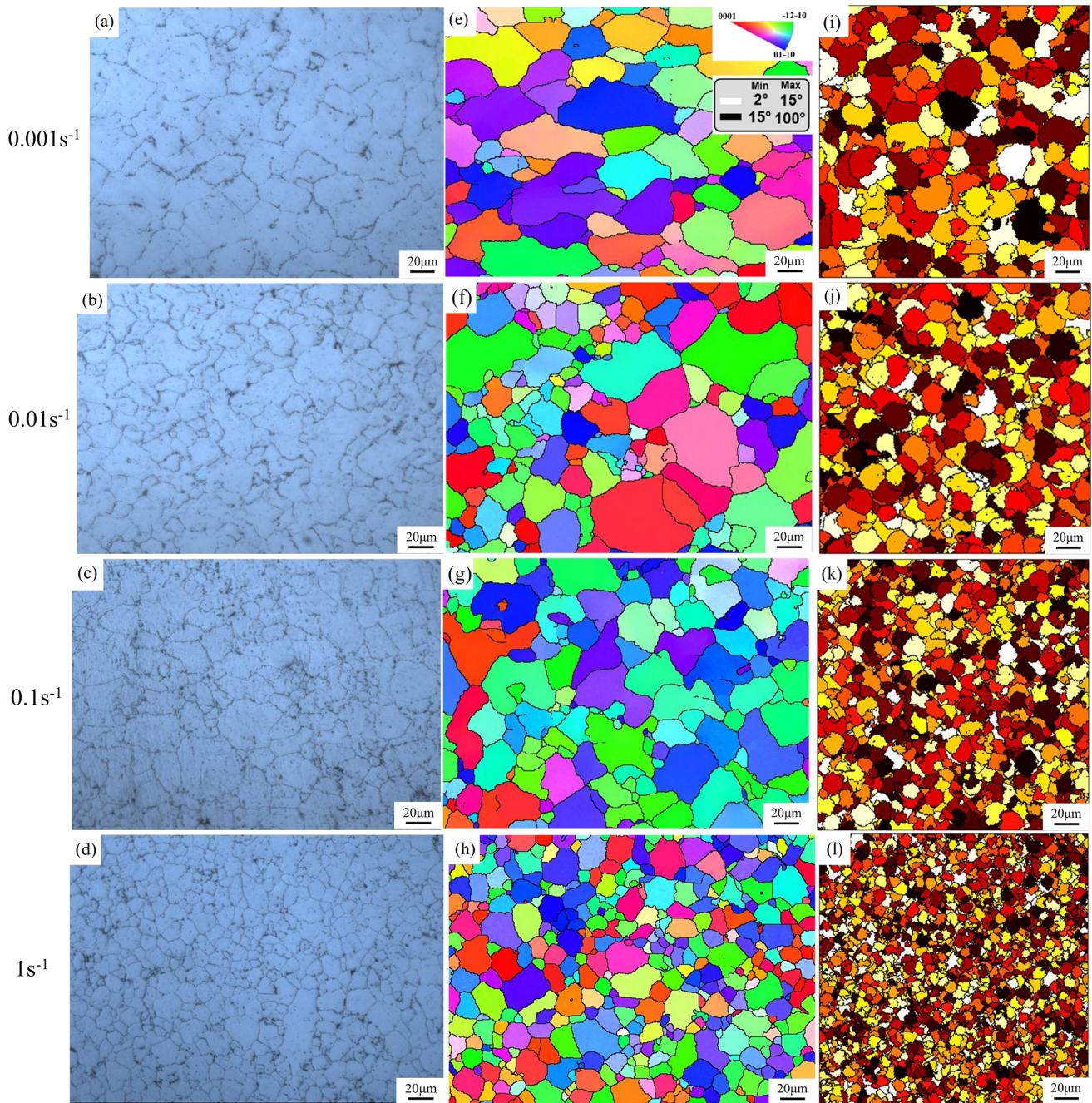
Figure 12 Microstructure of the middle region under different strain rates and the temperature of 673 K: **a**–**d** experiment; **e**–**h** EBSD maps; **i**–**l** simulation.

coupling FE method by DEFORM-3D and two-dimensional cellular automata (CA) is used for simulation. The material parameters required for CA simulation are shown in Table 2. The CA method adopts discrete time and space. The simulation area is 500 × 500 square cells with a size of 1 μm. The nucleation sites are randomly selected for nucleation. The initial microstructure based on the average grain size generated by the periodic

boundary condition simulation is shown in Fig. 10a. The average grain size is 43.6 μm, which has a very small variation of 0.6% compared with the experimentally measured average grain size.

To fully describe the DRX process (Fig. 10b), each cell in this CA model has five state variables: (1) The dislocation density variable represents the deformation energy storage. The dislocation density is the same
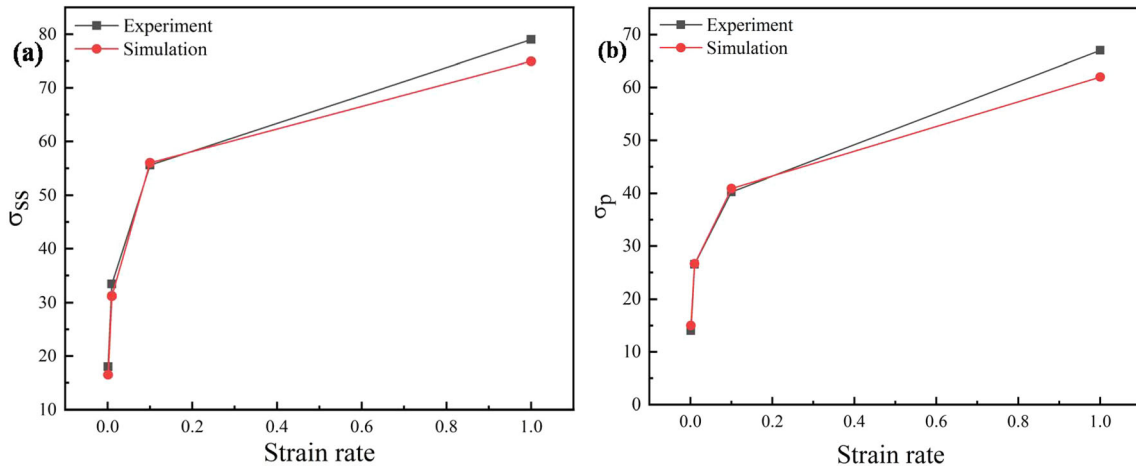
Figure 13 Comparison between experimental and simulated peak stress and steady-state stress at the temperature of 673 K and different strain rates. **a** Steady-state stress; **b** peak stress.

Table 3 Comparison of peak stress and steady-state stress data between experiment and CA simulation.

Temperature/K	Strain rate/s⁻¹	σ_p/MPa		σ_{ss}/MPa		Error (%)	
		Experiment	Simulated	Experiment	Simulated	σ_p	σ_{ss}
673	0.001	18.0	16.5	14.0	15.0	8.0	7.0
673	0.01	33.4	31.2	26.5	26.6	6.5	0.3
673	0.1	55.6	56.0	40.2	40.9	0.7	1.7
673	1	79.0	74.9	67.0	62.0	5.1	7.4

in different regions with an initial value of $\rho_{initial}$, which means that the dislocation is uniformly distributed. (2) The grain orientation variable is used to distinguish different grains. (3) The grain boundary variable represents whether the unit cell is located on the grain boundary. (4) The recrystallization fraction variable represents when the cell is recrystallized, which is set to 1. (5) The recrystallization time variable is used to track the recrystallization process.

The state change of each cell is determined by the state of its neighbors according to the corresponding transition rule. The flowchart of the CA and FE simulation of DRX is shown in Fig. 11. The flowchart mainly includes four parts: the import of FE deformation conditions; inputting material parameters; the generation of initial microstructure; and the prediction of DRX microstructure.

In DRX (Fig. 10b), non-recrystallized grains will be transformed into recrystallized grains after nucleation when the following conditions are met: (1) the unit cell is located on the grain boundary. (2) The driving force for the growth of the unit cell is positive. (3) The dislocation density (ρ) reaches a critical value (ρ_c), and as the dislocation density increases,

the possibility of cell nucleation increases. (4) The unit cell is generated according to the random number P ($P = m/4$), and the probability of recrystallization transformation, m, is the number of cells with the same orientation in the adjacent unit cells.

CA simulation results and discussions

Figure 12 shows the microstructures of experimental observation, EBSD maps, and CA model simulated in the middle region of the sample at the temperature of 673 K and strain rates of 0.001 s⁻¹, 0.01 s⁻¹, 0.1 s⁻¹, and 1 s⁻¹, respectively. Fine grains are obtained by the DRX process. Hence, the plastic deformation ability of the alloy is improved due to the softening by the DRX process. The strain corresponding to the middle region under different deformation conditions was derived from the FE method by DEFORM-3D and used as the input condition of the CA simulation to simulate its microstructure, as shown in Fig. 12. The CA simulated average grain size is 19.9 μm, 15.0 μm, 13.5 μm, and 9.6 μm, respectively. At the same time, the microstructure evolution of extruded AZ80A magnesium alloy during hot
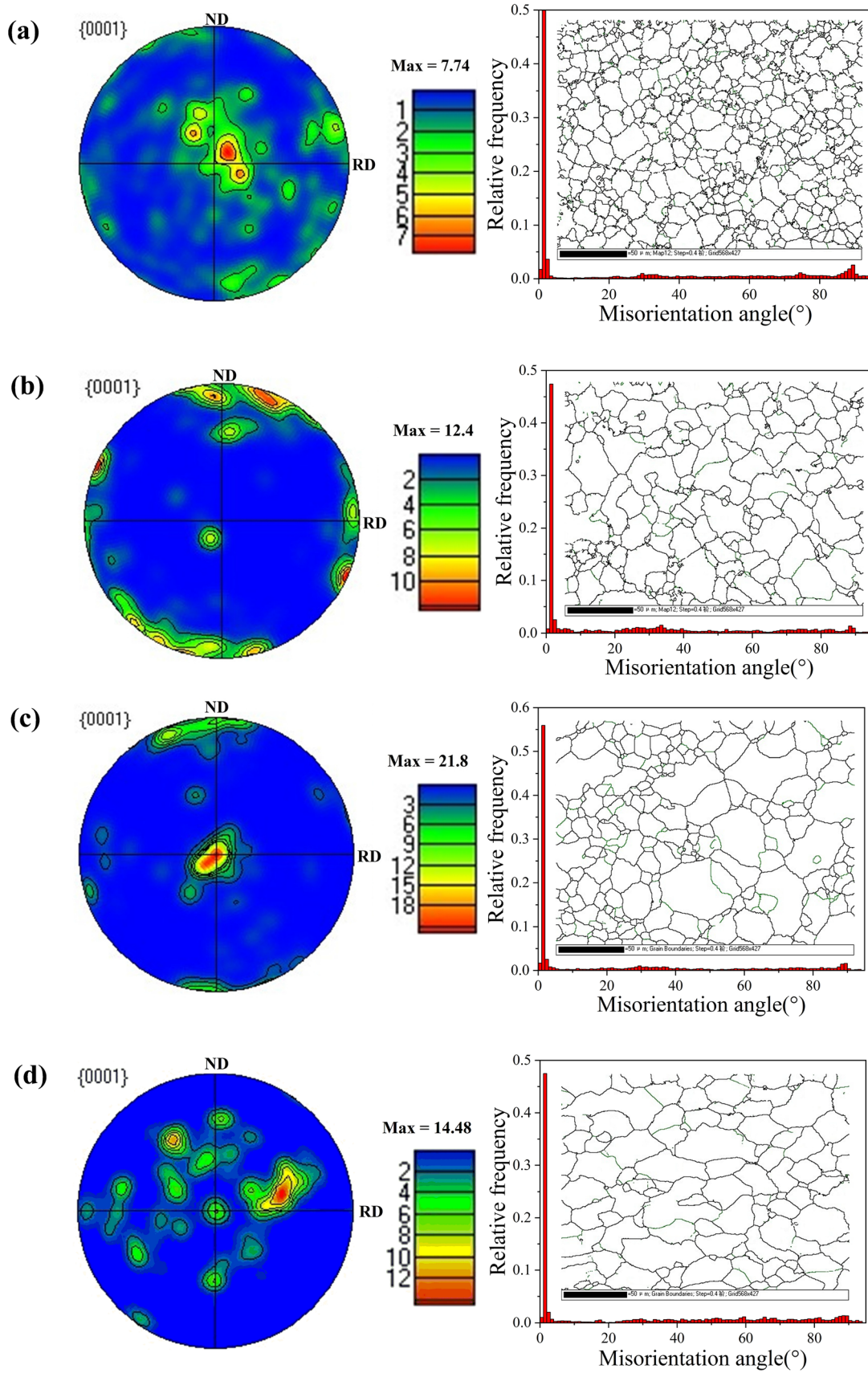
◄**Figure 14** Polar diagram, grain boundary diagram, and statistical diagram of grain boundary orientation difference of extruded AZ80A magnesium alloy under different deformation conditions. **a** 673 K–1 s^{-1}; **b** 673 K–0.1 s^{-1}; **c** 673 K–0.01 s^{-1}; **d** 673 K–0.001 s^{-1}.

compression was analyzed by EBSD, as shown in Fig. 12e–h, and the average grain size was 20.8 μm, 15.1 μm, 14.62 μm, and 10.3 μm. The error between CA simulation results and EBSD results is controlled by 8%, and the simulated microstructures under different deformation conditions are similar to the experimental results. The simulation results show that, at the same temperature, with the increase in the strain rate, the nucleation rate of DRX greatly increases, resulting in smaller average grain size. Figure 13 shows the comparison of peak stress and steady-state stress betsween the experiment and simulation results under different strain rates and a temperature of 673 K. Moreover, it reveals that the peak stress increases continuously with the increase in the strain rate. At the same time, Table 3 shows that the error between the peak stress simulated by CA and the experimental results is less than 8.0%. The simulation results are consistent with the experimental results, which indicates that the CA model can reliably predict the DRX behavior of the extruded AZ80A magnesium alloy.

Figure 14 shows the polar diagram, grain boundary diagram and statistical diagram of (0001) base plane grain boundary orientation difference at 673 K, strain 0.916, strain rate 1 s^{-1}, 0.1 s^{-1}, 0.01 s^{-1}, and 0.001 s^{-1}. The experiment was carried out at 673 K and 60% deformation. Twins are usually activated at low temperatures and small strains to coordinate deformation. At this temperature, a large number of non-base surface slips in magnesium alloys were opened, which led to cross slip and climb of a large number of dislocations, thus promoting the generation of recrystallization. Figure 12e–h shows that there are almost no (10–12) tensile twins in all samples. This is because when the deformation is 60%, complete dynamic recrystallization and new grain generation have occurred.

The < 0001 > pole diagram of Fig. 14a–d shows that under the condition that the strain rate is 1 s^{-1}, most of the base planes are around the CD direction, that is, the c axis of the grain is parallel to the CD (that is, perpendicular to the ND direction),

indicating that when the deformation rate is high, < a > basal slip is dominant. With the extension of deformation time, the recrystallized grains begin to grow. Figure 14b shows that the grains whose base plane is parallel to CD are easier to grow, and the surrounding grains whose base plane is perpendicular to CD are gradually absorbed. At the same time, Fig. 12g shows that the proportion of blue (<01–10>//CD) and green (<-12-10>//CD) grains increases significantly. During deformation under the condition of 0.01 s^{-1}, new grains are generated around the grown grains (as shown in Fig. 14c), and the base plane of most grains is rotated to the direction perpendicular to CD again, indicating that with the further increase in the deformation time, <0001> base plane slip has become the main DRX generation mechanism of the alloy again. At 0.001 s^{-1}, the maximum polar density of the base plane of the alloy decreases from 21.8 at 0.01 s^{-1} to 14.48, which means that the texture has been significantly weakened. According to the polar diagram (Fig. 14d), the base plane starts to shift to the area about 45°with CD, indicating that a large number of < c + a > pyramidal slips have occurred in the alloy. At this time, the DRX mechanism of the alloy is mainly base plane slip and cone slip.

The grain boundary diagram in Fig. 14a–d shows that the proportions of small-angle grain boundaries are 61.9%, 56.1%, 53.1% and 51.8%, respectively. The results show that with the increase in the strain rate, the small-angle grain boundary increase and the large-angle grain boundary decrease. The main reason is that the stacking fault energy of magnesium alloy is low. Under the condition of a high strain rate, the grains do not have enough time to nucleate, so the grain boundary cannot be migrated in a large amount.

CA method can simulate the DRX volume fraction of the extruded AZ80A magnesium alloy. The DRX volume fraction can also be calculated by the reduction in the flow stress by Eq. (11). The reliability of the prediction of the simulated results can be verified by comparing the DRX percentage simulated by the CA method and the experimental results.

Figure 15 shows the comparison of DRX volume fraction, flow stress curves, and average grain size predicted by CA simulation compared to experimental results at a constant temperature and different strain rates. It reveals that the predicted results are in good agreement with experimental results. In Fig. 15b, with the increase in the strain, a typical
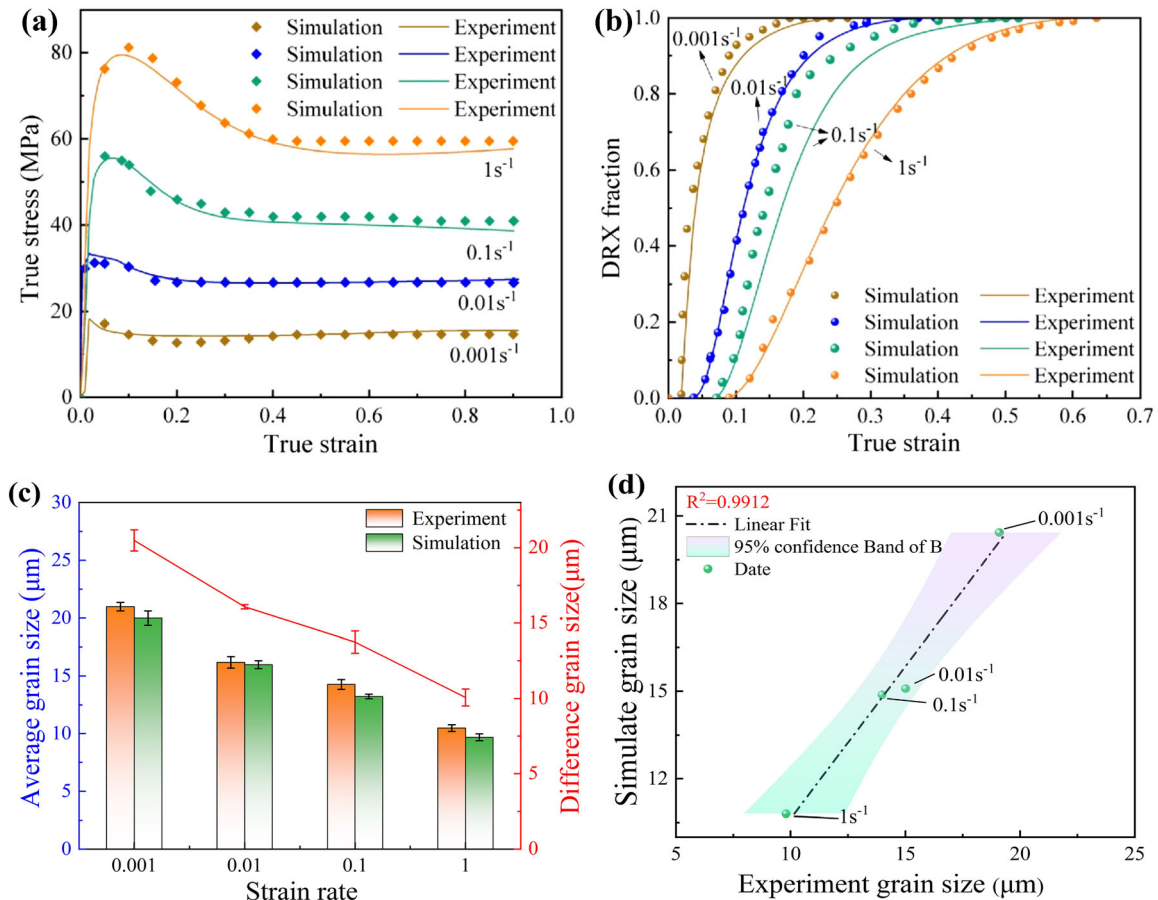
Figure 15 Comparison between the experiment and simulation results under different strain rates and the temperature of 673 K. **a** Flow stress curve; **b** DRX volume fraction; **c** grain size and error diagram; **d** comparison between the experiment and simulation results.

S-shaped curve shows the DRX kinetic process of the extruded AZ80A magnesium alloy. The S-shaped curve shows that, in the beginning, a very low DRX fraction is observed with slow growth. Then, the slow growth turns to rapid growth and finally to a stable value. This changing trend of the DRX process is consistent with the classic DRX kinetic model. As shown in Fig. 15a, the stress–strain curve shows that, at the beginning of thermal deformation, dynamic recovery (DRV) dominates. Due to the accumulation of dislocations during a further hot deformation, the strain will reach a critical value and the stacking fault energy will reach a critical value for the nucleation of DRX. When the deformation ratio continues to increase, the corresponding DRX volume fraction increases due to the nucleation and growth processes of DRX. When the work hardening and dynamic softening reach a balance, a stable flow stress stage can be observed. At this flow stress stage, the DRX volume fraction has a stable value, which is close to

100%. At the same temperature and strain conditions, the DRX volume fraction decreases with the increase in the strain rate. The stress–strain curve and DRX curve predicted by CA simulation are consistent with the experimental results. Moreover, the shapes of the nucleated grains in both the simulated and the experimentally observed cases are consistent. In summary, it is indicated that, when the strain rate decreases and the temperature increases, DRX nucleation is more likely to occur. Besides, complete development of the DRX fraction is almost reached when the flow stress curve reaches the steady state.

Figure 15c shows the average grain size and error diagram of experiments and simulations at different strain rates. The relative variations between the simulated data and the experimental data are 4.7%, 1.2%, 7.3%, and 7.5%, respectively. The average grain size decreases with the increase in the strain rate. The reason is that under the condition of a low strain rate, the longer deformation time and the increase in the

strain lead to the growth of recrystallized grains which are mainly nucleated at the grain boundaries of the original grains. Under the condition of a high strain rate, fine recrystallized grains are continuously generated at the original grain boundaries and recrystallized grain boundaries. However, the limited deformation time at a high strain rate cannot provide enough time for the growth of the recrystallized grains, resulting in the formation of a neckless of the small recrystallized grains surrounding the original grains. In Fig. 15d, the goodness of fit between the simulated and experimental values of the average grain size is 0.9912, and the relative error remains within 8%, which indicates the usefulness of the CA model simulation.

Figure 16 shows the microstructures under the deformation conditions of the strain rate of 0.01 s^{-1} and temperatures of 623 K, 673 K, and 723 K, which are compared with the microstructures predicted by CA simulation. The grain size distribution is also simulated by the CA method. From Fig. 16a, the DRX grain size is 11.02 μm at a low temperature. From Fig. 16b, when the temperature increases to 673 K, the DRX grains grow and the average grain size reaches 17.15 μm. As shown in Fig. 16c, the temperature continues to increase to 723 K, and the grain size increases to 22.64 μm. But, the average grain
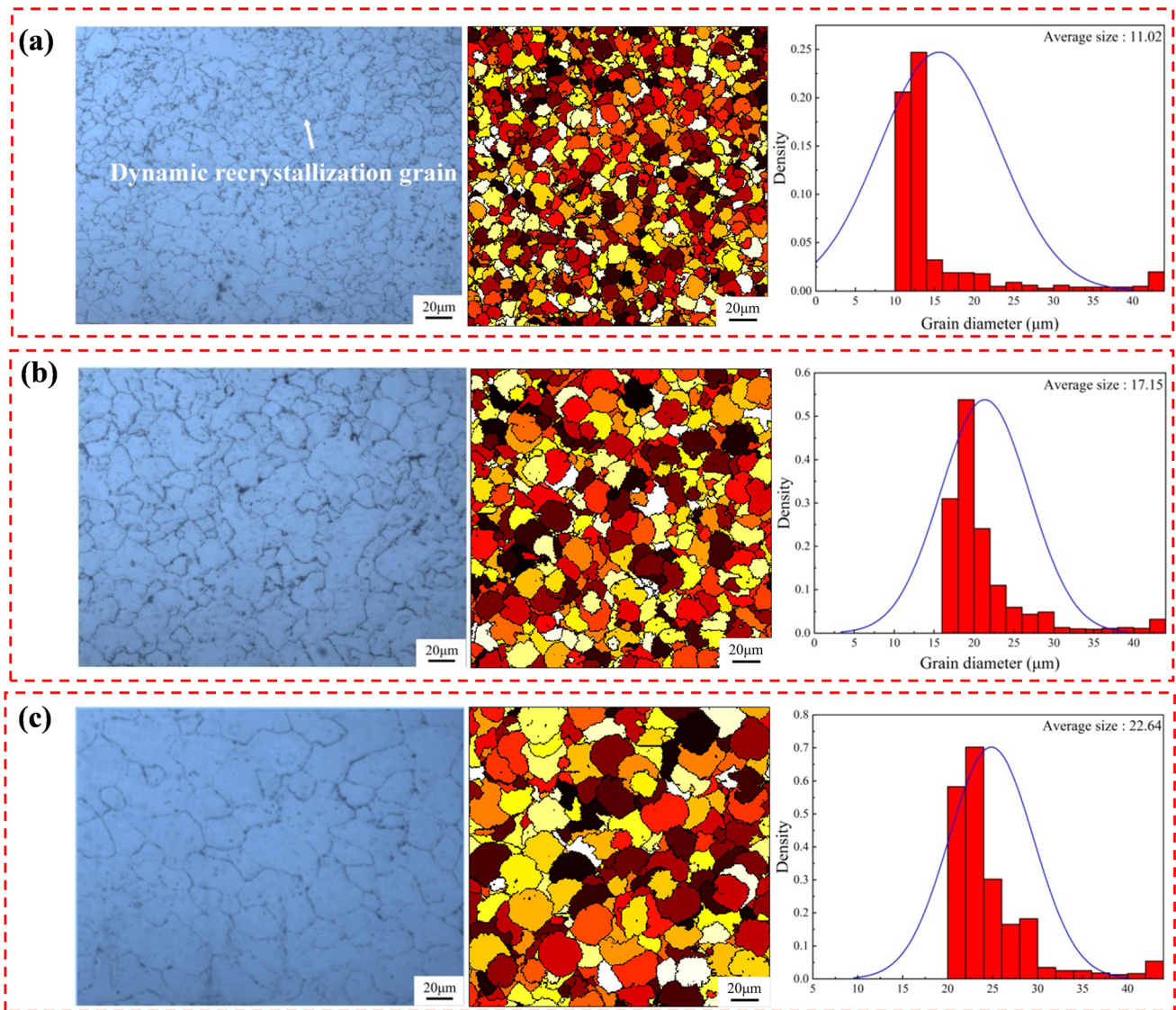

Figure 16 Comparison between experiment result and the CA predicted microstructure under the strain rate of 0.01 s^{-1} and temperature of 623 K, 673 K, and 723 K.

sizes are normally distributed at different temperatures. The average grain sizes obtained in the experiment are 9.76 μm, 16.53 μm, and 23.07 μm, respectively. The grain sizes predicted by the CA model are 11.02 μm, 17.15 μm, and 22.64 μm, respectively. The relative error is kept within 12%, which reveals that the experimental results are consistent with the simulated results. Therefore, the CA model can reliably simulate the microstructure of the extruded AZ80A magnesium alloy. Besides, it is concluded that the growth of the DRX grains is positively correlated with the increase in deformation temperature [36]. The reason is probably that the increase in deformation temperature contributes to the accumulation of dislocations, which directly influences the DRX process.

Figure 17 shows the microstructure diagrams of different strains ($\varepsilon = 0$, $\varepsilon = 0.05$, $\varepsilon = 0.15$, and $\varepsilon = 0.3$) simulated by the CA model at the strain rate of $0.01\ \mathrm{s}^{-1}$ and temperature of 623 K. DRX does not occur at the beginning of the thermal deformation. When the accumulated strain reaches a critical value of 0.05, as shown in Fig. 17b, the recrystallized grains begin to nucleate at the grain boundaries of the parent grains. As the strain increases to 0.15, as shown in Fig. 17c, the accumulated dislocation density promotes the occurrence of DRX, resulting in a rapid increase and growth of the recrystallized grains. When the strain increases to 0.3, the work hardening and dynamic softening reach an equilibrium state, as shown in Fig. 17d. At this strain, the DRX has completely occurred, and the DRX volume fraction
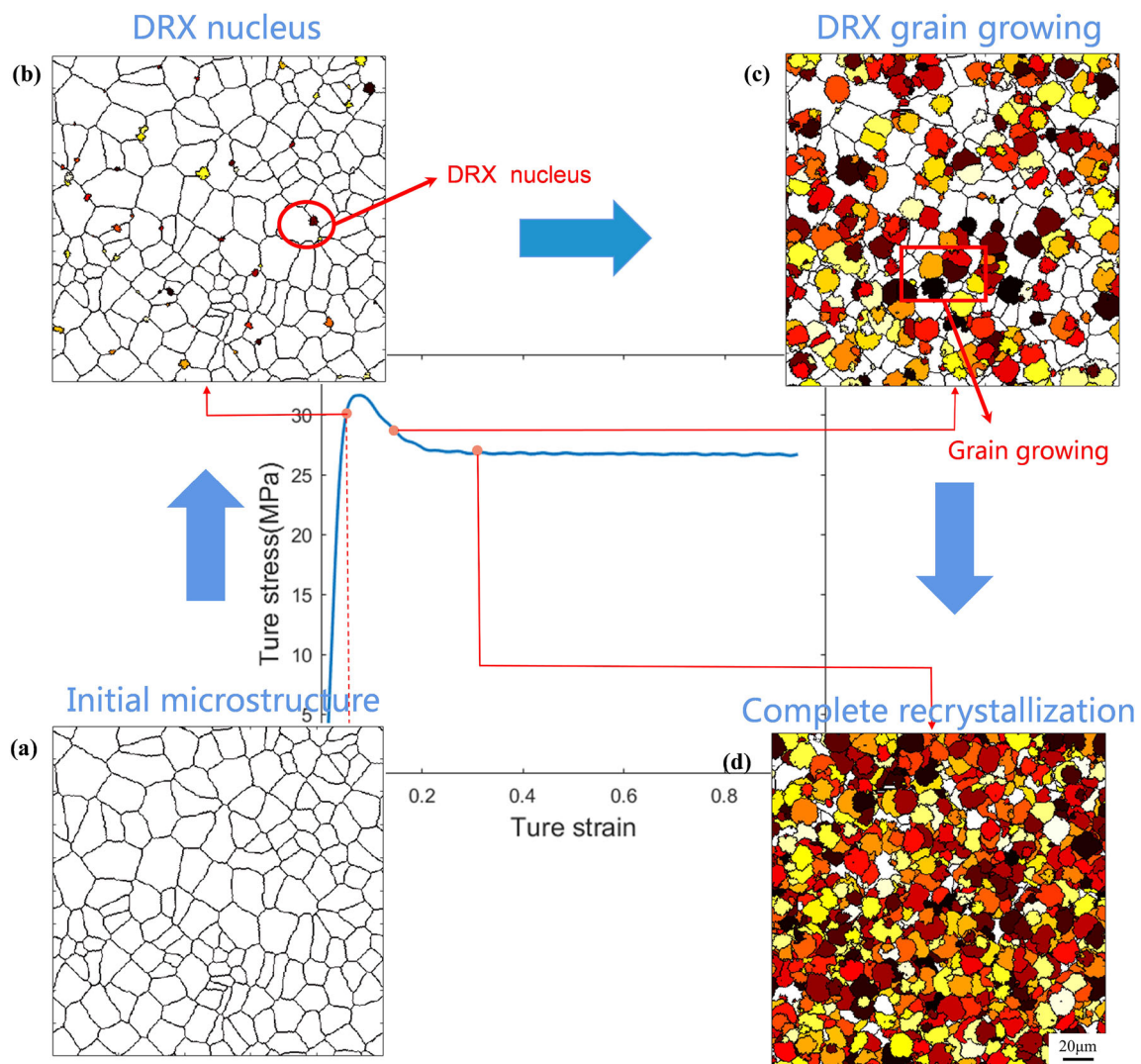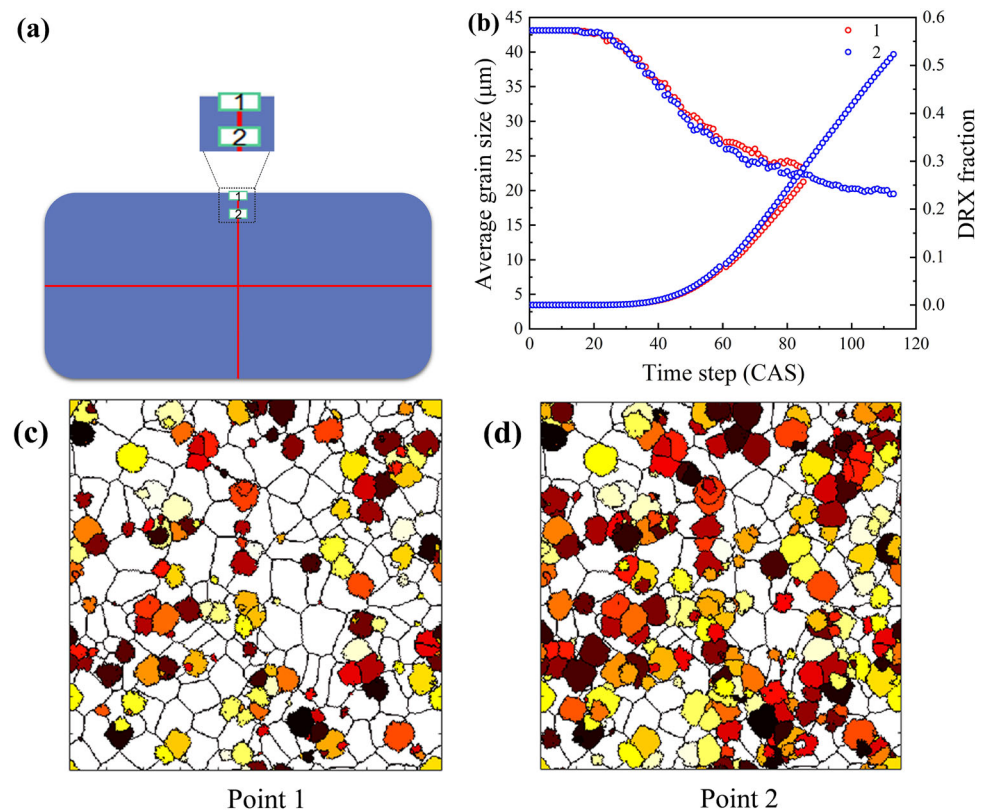

Figure 17 Microstructure under different strains at 623 K simulated by the CA method. **a** $\varepsilon = 0$; **b** $\varepsilon = 0.05$; **c** $\varepsilon = 0.15$; **d** $\varepsilon = 0.3$..

Figure 18 Changes in average grain size, DRX percentage, and microstructure of the sample close to the contact surface between the die and the sample.

Point 1   Point 2

reaches about 99%. Moreover, due to the large strain rate and short thermal deformation time, there is uneven nucleation in the process of the CA simulation.

Figure 18 shows the changes in average grain size, DRX percentage, and microstructure simulated by the CA method close to the contact surface of the sample between the die and the sample during isothermal compression. The strains of 0.09 and 0.12, respectively, corresponding to Point 1 and Point 2 are derived from the FE simulation by DEFORM-3D. These two strain values are used to import the CA simulated results to simulate the microstructural evolution in two different regions of the sample. As the number of simulation steps increases, the average grain size and DRX percentage of Point 1 and Point 2 are significantly different. The DRX percentage of Point 2 is much larger than that of Point 1. Figure 18c, d shows that, compared with Point 2, Point 1 has fewer nucleation spots in the beginning. With the increase in the time step and strain, the number of nucleation locations increases, resulting in a small

average grain size in Point 2. At the same time, grain refinement is achieved. The results show that a small location change in the sample leads to a significant change in the microstructure.

Conclusions

In this paper, a method based on the DRX-CA model and FE coupling is established to study the thermal deformation behavior of the extruded AZ80A magnesium alloy. This combined methodology is mainly used to analyze the effects of deformation parameters such as deformation temperature and strain rate on the microstructure. According to the simulation results, the conclusions are summarized as follows:

(1) The hot deformation activation energy of the extruded AZ80A magnesium alloy was 180 kJ/mol. The relationship between the Zener–Hollomon (Z) parameter and the peak stress (σ_P) was obtained:

$$Z = \dot{\varepsilon}\exp\left(-\frac{180000}{RT}\right)$$
$$= 3.30984 \times 10^{12}[\sinh(0.02016\sigma)]^{3.52062}$$

(2) The CA model was coupled with the FE model to simulate the microstructural evolution under different deformation conditions during thermal deformation. The simulated flow stress, grain size, and DRX volume fraction were verified by hot compression experiments. The DRX kinetic model of the extruded AZ80A magnesium alloy was expressed:

$$\begin{cases} X_{\mathrm{DRX}} = 0 & (\varepsilon \leq \varepsilon_{\mathrm{c}}) \\ X_{\mathrm{DRX}} = 1 - \exp\left[-0.17406\left(\dfrac{\varepsilon - \varepsilon_{\mathrm{c}}}{\varepsilon_{\mathrm{p}}}\right)^{2.0756}\right] & (\varepsilon \geq \varepsilon_{\mathrm{c}}) \end{cases}$$

(3) DRX behavior is the main mechanism during the hot compression of the extruded AZ80A magnesium alloy. The dislocation density model, grain growth, and nucleation model are established to provide the mathematical basis for DRX-CA simulation and to predict the microstructure under different deformation conditions. The errors between the flow stress and grain size predicted by the DRX-CA model and the experimental results are less than 8.0% and 11.0%, respectively, and the predicted DRX volume fraction presents an S-shaped curve, which are in good agreement with the experimental results, indicating that the model can reliably predict the microstructure of the extruded AZ80A magnesium alloy.

Acknowledgements

Declaration

Conflict of interest No conflict of interest exits in the submission of this manuscript, and manuscript is approved by all authors for publication. I would like to declare on behalf of my co-authors that the work described was original research that has not been published previously, and not under consideration for publication elsewhere, in whole or in part. All the authors listed have approved the manuscript that is enclosed.

References

[1] Chen Y, Hu L, Shi L et al (2020) Effect of texture types on microstructure evolution and mechanical properties of AZ31 magnesium alloy undergoing uniaxial tension deformation at room temperature. Mater Sci Eng A 769:138497

[2] Luo AA (2013) Magnesium casting technology for structural applications. J Magnes Alloys 1(1):2–22

[3] Park J, Kim J, Park N et al (2010) Study of forming limit for rotational incremental sheet forming of magnesium alloy sheet. Metal Mater Trans A 41(1):97–105

[4] Zhou G, Li Z, Li D et al (2017) A polycrystal plasticity based discontinuous dynamic recrystallization simulation method and its application to copper. Int J Plast 91:48–76

[5] Doherty R, Hughes D, Humphreys F et al (1997) Current issues in recrystallization: a review. Mater Sci Eng A 238(2):219–274

[6] Cram D, Zurob HS, Brechet Y et al (2009) Modelling discontinuous dynamic recrystallization using a physically based model for nucleation. Acta Mater 57(17):5218–5228

[7] Huang K, Logé RE (2016) A review of dynamic recrystallization phenomena in metallic materials. Mater Des 111:548–574

[8] Cai Y, Sun CY, Li YL et al (2020) Phase field modeling of discontinuous dynamic recrystallization in hot deformation of magnesium alloys. Int J Plast 133:102773

[9] Xiao N, Hodgson P, Rolfe B et al (2018) Modelling discontinuous dynamic recrystallization using a quantitative multi-order-parameter phase-field method. Comput Mater Sci 155:298–311

[10] Li J, Xu H, Mattila TT et al (2010) Simulation of dynamic recrystallization in solder interconnections during thermal cycling. Comput Mater Sci 50(2):690–697

[11] Chen F, Cui Z, Liu J et al (2010) Mesoscale simulation of the high-temperature austenitizing and dynamic recrystallization by coupling a cellular automaton with a topology deformation technique. Mater Sci Eng A 527(21–22):5539–5549

[12] Shabaniverki S, Serajzadeh S (2016) Simulation of softening kinetics and microstructural events in aluminum alloy subjected to single and multi-pass rolling operations. Appl Math Model 40(17–18):7571–7582

[13] Zhang H, Wang J, Chen Q et al (2019) Study of dynamic recrystallization behavior of T2 copper in hot working conditions by experiments and cellular automaton method. J Alloy Compd 784:1071–1083

[14] Ding R, Guo Z (2001) Coupled quantitative simulation of microstructural evolution and plastic flow during dynamic recrystallization. Acta Mater 49(16):3163–3175

[15] Han F, Chen RQ, Yang CH et al (2016) Cellular automata simulation on dynamic recrystallization of TA16 alloy during hot deformation. In: Mater Sci Forum, pp 245–250

[16] Chen F, Qi K, Cui Z et al (2014) Modeling the dynamic recrystallization in austenitic stainless steel using cellular automaton method. Comput Mater Sci 83:331–340

[17] Li H, Sun X, Yang H (2016) A three-dimensional cellular automata-crystal plasticity finite element model for predicting the multiscale interaction among heterogeneous deformation, DRX microstructural evolution and mechanical responses in titanium alloys. Int J Plast 87:154–180

[18] Wang Y, Peng J, Zhong L et al (2016) Modeling and application of constitutive model considering the compensation of strain during hot deformation. J Alloy Compd 681:455–470

[19] Lee HW, Im Y-T (2010) Numerical modeling of dynamic recrystallization during nonisothermal hot compression by cellular automata and finite element analysis. Int J Mech Sci 52(10):1277–1289

[20] De Jaeger J, Solas D, Fandeur O et al (2015) 3D numerical modeling of dynamic recrystallization under hot working: application to Inconel 718. Mater Sci Eng A 646:33–44

[21] Sellars CM, Mctegart W (1966) On the mechanism of hot deformation. Acta Metal 14(9):1136–1138

[22] Puchi-Cabrera ES, Guérin J-D, La Barbera-Sosa JG et al (2017) Incremental constitutive description of SAE 5120 steel deformed under hot-working conditions. Int J Mech Sci 133:619–630

[23] Puchi-Cabrera ES, Guérin J-D, La Barbera-Sosa JG et al (2018) Plausible extension of Anand's model to metals exhibiting dynamic recrystallization and its experimental validation. Int J Plast 108:70–87

[24] Lin Y, Chen X-M, Wen D-X et al (2014) A physically-based constitutive model for a typical nickel-based superalloy. Comput Mater Sci 83:282–289

[25] Wu B, Li M, Ma D (2012) The flow behavior and constitutive equations in isothermal compression of 7050 aluminum alloy. Mater Sci Eng A 542:79–87

[26] Hostos JA, Bencomo A, Cabrera EP et al (2018) Modeling the viscoplastic flow behavior of a 20MnCr5 steel grade deformed under hot-working conditions, employing a meshless technique. Int J Plast 103:119–142

[27] Xia Y, Zhang C, Zhang L et al (2017) A comparative study of constitutive models for flow stress behavior of medium carbon Cr–Ni–Mo alloyed steel at elevated temperature. J Mater Res 32(20):3875–3884

[28] Yi H-L, Wei D, Wang Y et al (2020) Hot deformation and dynamic recrystallization behavior of CoCrNi and (CoCrNi) 94Ti3Al3 medium entropy alloys. Metals 10(10):1341

[29] Mecking H, Kocks U (1981) Kinetics of flow and strain-hardening. Acta Metal 29(11):1865–1875

[30] Svoboda A, Wedberg D, Lindgren L-E (2010) Simulation of metal cutting using a physically based plasticity model. Model Simul Mater Sci Eng 18(7):075005

[31] Kurtz RJ, Abe K, Chernov V et al (2004) Recent progress on development of vanadium alloys for fusion. J Nucl Mater 329:47–55

[32] Wang L, Fang G, Qian L (2018) Modeling of dynamic recrystallization of magnesium alloy using cellular automata considering initial topology of grains. Mater Sci Eng A 711:268–283

[33] Roberts W, Ahlblom B (1978) A nucleation criterion for dynamic recrystallization during hot working. Acta Metal 26(5):801–813

[34] Liu Y-X, Lin Y, Li H-B et al (2015) Study of dynamic recrystallization in a Ni-based superalloy by experiments and cellular automaton model. Mater Sci Eng A 626:432–440

[35] Shen G, Hu B, Zheng C et al (2018) Coupled simulation of ferrite recrystallization in a dual-phase steel considering deformation heterogeneity at mesoscale. Comput Mater Sci 149:191–201

[36] Chen X, Liao Q, Niu Y et al (2019) A constitutive relation of AZ80 magnesium alloy during hot deformation based on Arrhenius and Johnson-Cook model. J Mater Res Technol 8(2):1859–1869